Algebraically solvable model for electron-phonon interactions in cycloacene molecules

D. Condado [*] and E. Sadurní [†]
Instituto de Física, Benemérita Universidad Autónoma de Puebla, Ciudad Universitaria, Puebla, Puebla 72570, México

R. A. Méndez-Sánchez [‡]
Instituto de Ciencias Físicas, Universidad Nacional Autónoma de México, Avenida Universidad s/n, Col. Chamilpa, Cuernavaca, Morelos 62210, México

(Received 22 August 2023; accepted 30 October 2023; published 27 November 2023)

The intrinsic polygonal symmetry of a [h]cycloacene molecule is employed to find the normal modes of the electronic and vibrational degrees of freedom using the interaction picture in a fixed molecule, i.e., without rotational degrees of freedom. Instead of considering separable solutions, the dynamics is studied implementing an electron-phonon linear coupling of first order. This coupling is described using an algebraic approach analogous to the Jaynes-Cummings model for atoms in optical cavities. Criteria for transitions are given based on the symmetry selection rules and conservation laws. A basis of electron-phonon dressed states is given and distortion phenomena usually associated with the Jahn-Teller effect in crystals are predicted.

DOI: 10.1103/PhysRevA.108.052823

I. INTRODUCTION

The Born-Oppenheimer approximation [1], which originated almost 100 years ago, has been for a long time a reliable tool to study the behavior of molecules since it greatly simplifies the complex equations that arise in multibody problems. Nowadays, however, it has become easier to deal with such systems by numerical methods [2–6]. The study of phenomena beyond this approximation, such as light-matter interaction and luminescence [7,8], has drawn attention for its influence in photophysical and photochemical processes and the potential fabrication of light-emitting diodes [9,10]. In the present work we introduce a coupling of nuclear observables to the electronic Hückel approximation in a linear fashion. By doing so, we obtain superpositions of terms algebraically equivalent to the Jaynes-Cummings model. This is done in a long organic molecule such as cycloacene. It should be noted that in this molecular context, the bosonic elements are attributed to the presence of phonons.

In contrast to the propagation of phonons in a periodic lattice in solid-state physics [11–13], here the medium of propagation of the phonons is the molecule itself. Hence there is no need for a cavity that traps the bosons in a cryogenic environment, as would be the case for the optical Jaynes-Cummings model [14]. This not only makes bosonic losses less frequent, it also offers the possibility of using the electron-phonon interaction for the creation of qubits; for systems that require ion traps, this is normally done with photon-exciton couplings [15,16]. The interaction between these degrees of freedom produces an effect analogous to fluorescence, in which an electronic state can transit either to a lower-energy state plus a vibrational excitation or to a higher-energy state by absorbing a quantum of vibration. In Fig. 1 we show a representation of this process. This implies that even an initial state with zero phonons can evolve into a state with vibrational excitations. Another effect expected from the coupling of electronic and vibrational degrees of freedom is the perturbation of the ground state such that the direct product of the lower electronic state and the zero-phonon vibrational state is not the state of minimal energy of the full system. In one-dimensional chains, this produces a Peierls distortion.

In this regard, we should mention that, according to our results, it is plausible to construct a two-level system with a cycloacene molecule of five rings; higher multilevel systems are also plausible and their prevalence increases with the size of the molecule. In addition, our treatment does not consider rotational degrees of freedom, as they are not involved in the motion. In regard to experimental realizations, the neutralization of rotations can be achieved with techniques such as nanopore trapping. Arrangements of this type have been demonstrated recently by experimentalists [17,18].

The structure of this article is as follows. In Sec. II we obtain the energy spectrum of the cycloacene molecule, with a procedure that has been employed previously [19,20], involving the polygonal symmetry of the molecule. We expand the scope of that study by implementing the vibrational degrees of freedom through a harmonic approximation and subsequently studying the linear coupling between the electronic transitions and the vibrational excitations: a task undertaken analytically for molecules of high complexity. In Sec. III A we rewrite the linear coupling in terms of the electronic and vibrational normal modes. Furthermore, in the same spirit as in the Jaynes-Cummings model for electromagnetic cavities, we implement the interaction picture and the rotating-wave

[*] dcondado@ifuap.buap.mx
[†] sadurni@ifuap.buap.mx
[‡] mendez@icf.unam.mx

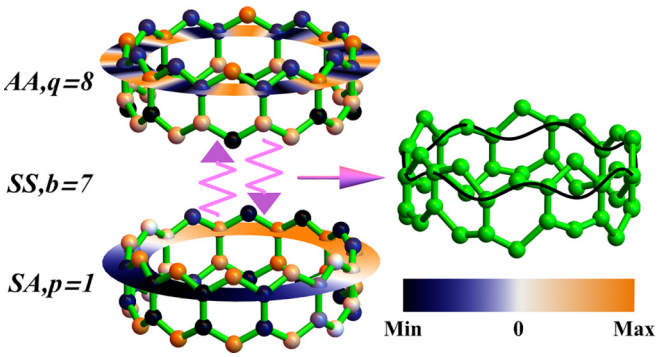

FIG. 1. Transition between the Hückel eigenstates $|AA, 8\rangle$ and $|SA, 1\rangle$ mediated by a phonon with frequency ω_7^{SS} along the $\hat{z}$ axis. The eigenstates and frequencies are defined in (17) and (21), respectively

approximation to obtain stationary solutions. In Sec. III B we discuss the existence of various selection rules that filter the possible electron-phonon couplings beyond the conservation of energy with criteria that involve conservation of parity and Bloch momentum. In Sec. III C we introduce physical values of molecular parameters to obtain viable realizations in cycloacene. Some notorious examples are detailed in Sec. III D, where the dynamics involve systems of two, three (here we mention how a Peierls distortion is possible), and four interacting electronic levels. Solutions to these systems are given in the form of dressed states. In Sec. IV we discuss the implications of the obtained results.

II. MATHEMATICAL MODEL OF A CYCLOACENE MOLECULE

We know that for organic compounds, the σ bonds that keep each carbon atom connected to the molecule originate from a basis of hybridized sp^2 orbitals, which is orthogonal to the remaining delocalized π orbital. For this reason, the Hamiltonian can be split into a term that operates in the basis of the atoms' π orbitals H_E and a term that involves the dynamics of the molecule's σ bonds H_v:

$$H = H_E + H_v. \tag{1}$$

We note that, in the basis of the sp^2 orbitals, H_E is degenerate per carbon atom, thus allowing us to consider the same potential for all carbon-carbon interaction. This is equivalent to implementing the Born-Oppenheimer approximation for the dynamics in the σ bonds, but in the following we go beyond this approximation for H_E. The Hückel model will be implemented for H_E and a harmonic approximation will enable a normal-mode description of H_v. We may also refer to the π orbitals as the electronic degrees of freedom and the nuclear observables as the vibrational degrees of freedom.

The segmentation of periodic systems is an effective technique to deduce the eigenvalues of their Hamiltonians [20–22]. Proceeding in this manner, in Fig. 2(a) we define the coordinate system and show the segmentation of the cycloacene molecule (light shade) in identical units (darker shade) and for the sake of clarity, in the following we will refer to these units as benzene rings. In Fig. 2(b), in the context of the carbon atoms' π orbitals (see Sec. II A), we see how each benzene ring is labeled by index i, which ranges from 1 to h. Due to the periodicity of the system, it is possible to employ the i mod$h$ notation. We also use two pairs of numbers (1 and 2) to label the positions of the four atoms in each ring: The first number indicates if the atom is located in either the superior (1) or inferior (2) chain and the second number indicates if the atom is located in either an odd (1) position (meaning that in these places, the superior and inferior chains are coupled) or an even (2) position (here the superior and inferior chains are not coupled). This position label will be shortened with a single symbol $w = 11, 12, 21, 22$. Our notation will also be employed to label the atomic position vectors. With this, we can write the explicit Hamiltonians of the system in the next section.

A. Electronic Hamiltonian

The energy levels available to a single electron can be studied through the electronic Hamiltonian H_E below. To that end, we assume that, due to hybridization of the orbitals, each carbon atom has a π orbital available, which implies that all σ orbitals are occupied. These are the requirements needed for the applicability of the Hückel model [23–25]. Additionally, the local radial wave function $\mathscr{R}$ for each carbon atom is

$$\mathscr{R}(r) = \mathscr{N} r e^{-r/\lambda}, \quad \lambda = \frac{2a_0}{Z}, \; Z = 6. \tag{2}$$

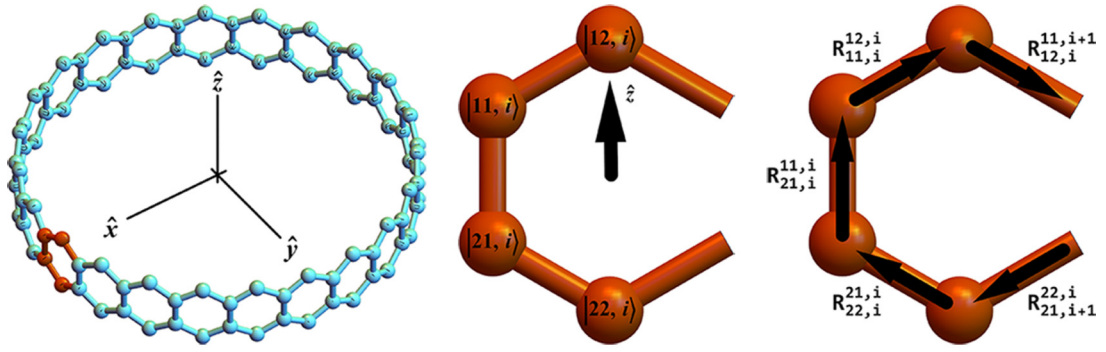

(a) (b) (c)

FIG. 2. Diagram and labeling of a [23] cycloacene molecule. (a) Coordinate system definition and segmentation of the molecule. (b) Four C atoms per hexagonal cell and their π-orbital states. (c) Five relative vectors between nearest-neighbor C atoms per hexagonal cell.

We should note that the constant evanescence length λ is one order of magnitude smaller than the equilibrium separation R between nearest neighbors $\lambda/R \approx 0.127$. For this reason, we consider a tight-binding model up to nearest neighbors. The same considerations are occasionally made for the analysis of the electronic structure of benzene beyond nearest-neighbor tight-binding models [26]. In this fashion, the electronic Hückel Hamiltonian is given by the expression

$$H_E = E_0 \sum_{\text{all } w} \left(\sum_{i=1}^{h} |w,i\rangle \langle w,i| + \sum_{\prec w,i;w',j\succ} \Delta^{w,i}_{w',j} |w,i\rangle \langle w',j| \right),$$

$$\Delta^{w,i}_{w',j} = \langle w,i|H_E|w',j\rangle \approx \Delta(R) e^{-|\mathbf{r}_i^w - \mathbf{r}_j^{w'}|/\lambda}, \tag{3}$$

where the notation $\prec w,i;w',j\succ$ indicates a sum carried over nearest neighbors, $\mathbf{r}_i^w$ are the position vectors of the carbon atoms, $\Delta(R)$ is the hopping amplitude at $\mathbf{r}_i^w = \mathbf{r}_j^{w'}$ (nearest neighbors), and $|w,i\rangle$ are the electronic π-orbital site kets of the carbon atoms; such orbitals are shown in Fig. 2(b). We note that there are only off-diagonal corrections due to ionic displacements; the lack of on-site oscillator contributions can be justified as explained in Appendix B. Furthermore, we can separate the electronic Hamiltonian by expanding the exponential function about the equilibrium configuration of the molecule,

$$d^{w,i}_{w',j} = \left|\mathbf{r}_i^w - \mathbf{r}_j^{w'}\right|, \quad \mathbf{R}^{w,i}_{w',j} = \mathbf{R}_i^w - \mathbf{R}_j^{w'}, \quad \left|\mathbf{R}^{w,i}_{w',j}\right| = R,$$

$$e^{-d^{w,i}_{w',j}/\lambda} \approx e^{-R/\lambda} + \frac{\partial}{\partial d^{w,i}_{w',j}} e^{-d^{w,i}_{w',j}/\lambda}\bigg|_{d^{w,i}_{w',j}=R} \left(d^{w,i}_{w',j} - R\right)$$

$$\approx e^{-R/\lambda}\left(1 - \frac{1}{\lambda}\hat{\mathbf{R}}^{w,i}_{w',j} \cdot \mathbf{r}^{w,i}_{w',j}\right), \tag{4}$$

where $\mathbf{R}_i^w$ are the atomic position vectors in the molecule's equilibrium configuration and $\mathbf{r}^{w,i}_{w',j}$ is defined in (9). In Fig. 2(c) we show how vectors $\mathbf{R}^{w,i}_{w',j}$ form a regular hexagon minus one edge in each benzene ring and that the number of edges is the same as the number of terms in the sum over nearest neighbors ($5h$). We stress that this interaction of the π orbitals with an ionic lattice does not follow the Born-Oppenheimer approximation. In Appendix A we show explicit forms of these sums. In this fashion, we can separate the electronic Hamiltonian as

$$H_E - E_0 = H_e + H_i, \tag{5}$$

$$H_e = \Delta_0 \left(\sum_{\prec w,i;w',j\succ} |w,i\rangle \langle w',j| + \text{H.c.} \right), \tag{6}$$

$$H_i = -\frac{1}{\lambda}\Delta_0 \sum_{\prec w,i;w',j\succ} \left(\hat{\mathbf{R}}^{w,i}_{w',j}\right)^T \mathbf{r}^{w,i}_{w',j} |w,i\rangle \langle w',j| + \text{H.c.}, \tag{7}$$

where $\Delta_0 = e^{-R/\lambda}\Delta(R)$ is the first-neighbor coupling energy at equilibrium. It is important to give an interpretation of each term: H_e is the untangled electronic Hamiltonian and H_i is our interaction Hamiltonian, since this operator couples the electronic and vibrational degrees of freedom. We will see that there can be energy transfers between these degrees of freedom via a phenomenon analogous to the Jaynes-Cummings effect in an optical cavity. It should be noted that the first neighbor coupling Δ_0 can vary in a certain atomic site if such a carbon atom is saturated with a radical other than hydrogen, e.g., fluorination [27,28]. This would change the overall ground state of the system as well as the highest-energy level, thus affecting the results we present. For this reason, we leave this possibility for future consideration.

It is important to note that even though we have made an attempt to derive the interaction terms from a well-justified Hamiltonian, it is always possible to propose an expression similar to (7) on the grounds of the simplest interaction model between electrons and phonons in the harmonic approximation, thus always linear in the nuclear coordinates. This would entail the use of an empirical coupling constant that could be fitted by spectroscopic data [29,30]; however, our approach checks with experiments of microwave emission and absorption in the vibronic part, i.e., the constant has the correct order of magnitude and a reasonable dependence on internuclear distance and evanescent length, taken from an effective Bohr radius for C atoms.

B. Vibrational Hamiltonian

For the vibrational Hamiltonian H_v we consider a harmonic interaction given by

$$H_v = \frac{1}{2m} \sum_{\text{all } w} \sum_{i=1}^{h} \left(\mathbf{p}_i^w\right)^2 + V_{\text{har}}, \tag{8}$$

$$V_{\text{har}} = \frac{1}{2}k \sum_{\prec w,i;w',j\succ} \left(\mathbf{r}^{w,i}_{w',j}\right)^2, \quad \mathbf{r}^{w,i}_{w',j} = \mathbf{r}_i^w - \mathbf{r}_j^{w'} - \mathbf{R}^{w,i}_{w',j}, \tag{9}$$

where the notation $\prec w,i;w',j\succ$ once more indicates a sum carried over nearest neighbors, m is the mass of the carbon atom, the bond force constant k can be determined from spectroscopy (see Sec. III C), and $\mathbf{p}_i^w$ are the momentum vectors of the carbon atoms. For a model closer to reality, instead of the harmonic approximation, we can propose an algebra based on f oscillators that allows for a description beyond the harmonic oscillator [31,32].

C. Solutions of the uncoupled systems

The diagonalization of the untangled electronic Hamiltonian H_e and the vibrational Hamiltonian H_v not only yields the energy eigenvalues of the uncoupled systems, but also enables us to work with their eigenbases, which allows us to write

$$H_e = \hbar \sum_{\text{all } Q} \sum_{q=1}^{h} \nu_q^Q \sigma_{qq}^{QQ}, \quad \sigma_{qp}^{QP} = |Q,q\rangle(P,p|, \tag{10}$$

$$H_v = (4h)^2 \frac{\mathbf{p}^2_{\text{c.m.}}}{2M_T} + \sum_{\text{all } W} \sum_{q=1}^{h} \hbar\omega_q^W \left(\boldsymbol{a}_q^{W\dagger}\boldsymbol{a}_q^W + \frac{3}{2}\right), \tag{11}$$

where $|Q,q\rangle$ is an eigenstate of H_e (in the following, these states will be derived as linear combinations of the orbital kets $|w,i\rangle$); $\mathbf{p}_{\text{c.m.}}$ is the momentum of the center of mass of the molecule; M_T is its total mass (ignoring the masses of the hydrogen atoms); $\boldsymbol{a}_q^W$ and $\boldsymbol{a}_q^{W\dagger}$ are the annihilation and creation operators associated with the absorption and production

of phonons, respectively; Q, P, and W are symmetry labels which will be explained thoroughly in Sec. II C 1; and indices q and b are the Bloch momenta of the electronic and vibrational states, respectively. In this context, a Bloch momentum represents the propagation of the wave function throughout the molecule in a fashion analogous to the propagation vector of photons in a continuum. In Fig. 1 we can visualize this propagation as the periodicity of the waves.

Translational symmetry greatly simplifies the procedure of finding the eigenstates of a periodic system, e.g., a crystalline arrangement. Here we use the inherent C_h rotational symmetry of the molecule to our favor. It will prove useful to remember that the matrix representation of this group allows a diagonalization through the following basis:

$$(M)_{rc} = \frac{1}{\sqrt{h}} e^{i(2\pi/h)rc}. \tag{12}$$

1. Diagonalization of the untangled electronic Hamiltonian

The notation introduced in Sec. II A uses three numbers to label the atoms in the molecule. Likewise, we will employ direct products of three operators

$$O_1 O_2 O_3 \tag{13}$$

to write the untangled electronic Hamiltonian. Following the labeling shown in Fig. 2(b), both O_1 and O_2 have a 2×2 matrix representation: O_1 includes all four permutations between the upper and lower rows of each benzene ring (including the identity operations), while O_2 does the same for the even and odd positions of the carbon atoms. Finally, O_3 has an $h \times h$ representation and accounts for the benzene ring label. Now we write the untangled electronic Hamiltonian H_e as

$$\begin{aligned}
H_e/\Delta_0 &= P_2(\sigma_+ T^\dagger + \sigma_- \mathbf{1}_h) + \sigma_+ P_1 \mathbf{1}_h + P_1(\sigma_+ \mathbf{1}_h + \sigma_- T) + \text{H.c.} = \mathbf{1}(\sigma_+ K^\dagger + \sigma_- K) + \sigma_1 P_1 \mathbf{1}_h, \\
P_1 &= |1\rangle\langle 1|, \quad P_2 = |2\rangle\langle 2|, \quad \sigma_+ = |1\rangle\langle 2|, \quad \sigma_- = |2\rangle\langle 1|, \\
\mathbf{1} &= P_1 + P_2, \quad \sigma_1 = \sigma_+ + \sigma_-, \quad \sigma_3 = P_1 - P_2, \\
\mathbf{1}_h &= \sum_{i=1}^{h} |i\rangle\langle i|, \quad T = \sum_{i=1}^{h-1} |i\rangle\langle i+1| + |h\rangle\langle 1|, \quad K = \mathbf{1}_h + T.
\end{aligned} \tag{14}$$

We can write the matrix representation in the site basis of this operator as

$$H_e = \Delta_0 \left(\begin{array}{cc|cc} 0 & K^T & I_h & 0 \\ K & 0 & 0 & 0 \\ \hline I_h & 0 & 0 & K^T \\ 0 & 0 & K & 0 \end{array}\right), \quad K = \begin{pmatrix} 1 & 1 & 0 & \cdots & 0 \\ 0 & 1 & 1 & \cdots & 0 \\ \vdots & \vdots & \vdots & \ddots & \vdots \\ 1 & 0 & 0 & \cdots & 1 \end{pmatrix}, \tag{15}$$

where I_h is the $h \times h$ identity matrix. From (13) we recognize that in this conjunct $4h \times 4h$ matrix representation, the operator O_1 determines the places of the four outer blocks (separated by lines). Likewise, the operator O_2 determines the places of the four subblocks contained inside the previous blocks. Finally, the entries of these subblocks are the representations of operator O_3. In the same fashion, we can diagonalize H_e by employing three unitary transformations

$$\begin{aligned}
V_1 &= \frac{1}{\sqrt{2}} \begin{pmatrix} \mathbf{1} & 0 & \mathbf{1} & 0 \\ 0 & \mathbf{1} & 0 & \mathbf{1} \\ \mathbf{1} & 0 & -\mathbf{1} & 0 \\ 0 & \mathbf{1} & 0 & -\mathbf{1} \end{pmatrix}, \quad V_2 = \begin{pmatrix} M & 0 & 0 & 0 \\ 0 & M & 0 & 0 \\ 0 & 0 & M & 0 \\ 0 & 0 & 0 & M \end{pmatrix}, \\
V_2^\dagger V_1^\dagger H_e V_1 V_2 &= \begin{pmatrix} \mathbf{1} & D^\dagger & 0 & 0 \\ D & 0 & 0 & 0 \\ 0 & 0 & -\mathbf{1} & D^\dagger \\ 0 & 0 & D & 0 \end{pmatrix}, \quad (D)_{qp} = \delta_{qp}(1 + e^{i2\pi q/h}),
\end{aligned} \tag{16}$$

where δ_{qp} is a Kronecker delta. It is now evident that $V_2^\dagger V_1^\dagger H_e V_1 V_2$ can be diagonalized with the same ease as two 2×2 matrices. We thus arrange a final V_3 such that

$$\begin{aligned}
&V = V_1 V_2 V_3, \quad V^\dagger H_e V = \hbar \boldsymbol{\nu}, \quad H_e|Q,q) = \hbar \nu_q^Q |Q,q), \quad \boldsymbol{\nu} = \text{diag}(\boldsymbol{\nu}^{SS}, \boldsymbol{\nu}^{SA}, \boldsymbol{\nu}^{AS}, \boldsymbol{\nu}^{AA}), \quad (\boldsymbol{\nu}^Q)_{qp} = \delta_{qp} \nu_q^Q, \\
&\nu_q^{SS} = \nu_q^+, \quad \nu_q^{SA} = \nu_q^-, \quad \nu_q^{AS} = -\nu_q^-, \quad \nu_b^{AA} = -\nu_b^+, \quad \nu_q^\pm = \delta_{qp} \frac{\Delta_0}{2\hbar} \left[1 \pm \sqrt{1 + 16 \cos^2\left(\frac{\pi q}{h}\right)} \right], \quad \Delta_0 < 0,
\end{aligned} \tag{17}$$

where $\boldsymbol{\nu}$ is $4h \times 4h$ and $\boldsymbol{\nu}^Q$ is $h \times h$. Here we employ labels $Q, P = SS, SA, AS, AA$ to classify the normal electronic modes according to their symmetries in the following manner. As can be inferred from Fig. 2(a), the system is invariant under parity in the $\hat{z}$ axis. Thus all states must be either symmetric or antisymmetric under this operation. In particular, $|SS,q)$ and $|SA,q)$ [$|AS,q)$ and $|AA,q)$] are the symmetric (antisymmetric) eigenstates of this symmetry operation, i.e., we refer to the first symbol. Moreover, it is possible to define a unitary operation $\hat{\pi}_s$ such that $\hat{\pi}_s^2 = 1$, $\pi_s|Q,q) = |Q,q)$

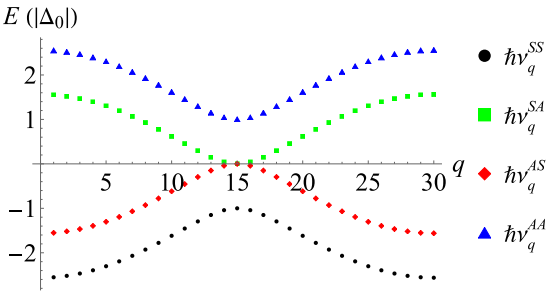

FIG. 3. Electronic spectrum of a cycloacene molecule with 30 benzene rings in terms of $|\Delta_0|$. It consists of four bands with 30 energy values; their explicit forms follow from (17).

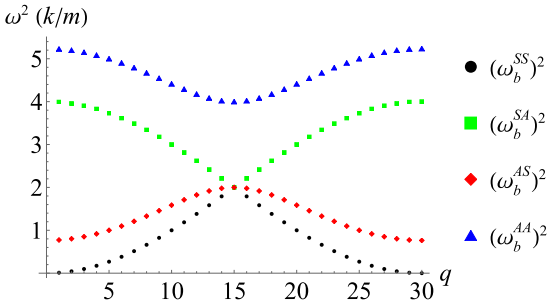

FIG. 4. Squared vibrational spectrum of a cycloacene molecule with 30 benzene rings in terms of k/m. As in the electronic case, it consists of four bands with 30 energy values; their explicit forms follow from (21).

for $Q = SS, AS$, and $\pi_s|Q, q) = -|Q, q)$ for $Q = SA, AA$, thus allowing us to complete the labeling according to the symmetries. This last operation is neither a parity nor a permutation between orbitals; however, it is approximately a permutation between even and odd sites in the limit where the superior and inferior chains are decoupled.

The energy spectrum of a cycloacene molecule with $h = 30$ benzene rings is shown in Fig. 3. It should be noted that the coefficients for the change of bases are given by

$$\langle w, i|Q, q) = V_{iq}^{wQ}, \quad (P, p|j, w'\rangle = \left(V_{jp}^{w'P}\right)^*. \tag{18}$$

2. *Diagonalization of the vibrational Hamiltonian*

The diagonalization of (8) is equivalent to finding the vibrational modes of the classical molecule. We begin by organizing the position vectors into a single position column (though for ease in the notation we show the transpose counterparts):

$$\mathbf{r}^T = \left(\left\{\left(\mathbf{r}_i^{11}\right)^T\right\}, \left\{\left(\mathbf{r}_i^{12}\right)^T\right\}, \left\{\left(\mathbf{r}_i^{21}\right)^T\right\}, \left\{\left(\mathbf{r}_i^{22}\right)^T\right\}\right),$$
$$\left\{\left(\mathbf{r}_i^{w}\right)^T\right\} \equiv \left(\left(\mathbf{r}_1^{w}\right)^T, \ldots, \left(\mathbf{r}_h^{w}\right)^T\right), \quad \mathbf{r}_i^w \cdot \hat{x}_k = r_{ik}^w. \tag{19}$$

Here the labels of the position vectors are the same implemented for the orbital site kets $|w, i\rangle$ and the index k represents the Cartesian component. Note that we can analogously define a conjoint momentum column $\mathbf{p}$ canonically conjugate to $\mathbf{r}$. With this notation, we can write the harmonic potential V_{har} as

$$V_{\text{har}}/k = \mathbf{r}^T A \mathbf{r} + \mathrm{b}^T \mathbf{r} + 5hR^2/2 = \tilde{\mathbf{r}}^T A \tilde{\mathbf{r}} + V_0/k, \quad \tilde{\mathbf{r}} = \mathbf{r} + \boldsymbol{\alpha},$$
$$2\boldsymbol{\alpha}^T A = \mathrm{b}^T, \quad V_0 = 5hR^2/2 - \boldsymbol{\alpha}^T A \boldsymbol{\alpha},$$
$$A = \frac{1}{2}\begin{pmatrix} 3I_h & -K^T & -I_h & 0 \\ -K & 2I_h & 0 & 0 \\ -I_h & 0 & 3I_h & -K^T \\ 0 & 0 & -K & 2I_h \end{pmatrix} \otimes \mathbf{1}_{3\times 3}. \tag{20}$$

Here the 3×3 identity represents the components of position vectors in Cartesian coordinates and $\boldsymbol{\alpha}$ are the constant position vectors that enable us to complete the square; it is possible to prove that $V_0 = 0$.

We note how this matrix is very similar to (15), which is not surprising since both the electronic and vibrational Hamiltonians have the same C_h symmetry. Its diagonalization follows the same steps we implemented with H_e (only the third unitary matrix is different):

$$U = V_1 V_2 U_3, \quad U^\dagger A U = \frac{m}{2k}\boldsymbol{\omega}^2,$$
$$\boldsymbol{\omega} = \mathrm{diag}(\boldsymbol{\omega}^{SS}, \boldsymbol{\omega}^{SA}, \boldsymbol{\omega}^{AS}, \boldsymbol{\omega}^{AA}), \quad (\boldsymbol{\omega}^W)_{bd} = \delta_{bd}\omega_b^W,$$
$$\omega_b^{SS} = \omega_b^-, \quad \omega_b^{SA} = \omega_b^+, \quad \omega_b^{AS} = \Omega_b^-, \quad \omega_b^{AA} = \Omega_b^+,$$
$$\omega_b^\pm = \sqrt{2(k/m)[1 \pm |\cos(\pi b/h)|]}$$
$$\Omega_b^\pm = \sqrt{(k/m)[3 \pm \sqrt{4\cos^2(\pi b/h) + 1}]}. \tag{21}$$

Here the symmetry classification W of the normal modes of vibration is analogous to the classification Q of the electronic modes. In Fig. 4 we can appreciate the normal frequencies of vibration of a cycloacene molecule with 30 benzene rings. Given that we are using a harmonic approach, the definition of the following creation and annihilation operators is expected:

$$\boldsymbol{\eta} = U^\dagger \tilde{\mathbf{r}}, \quad \boldsymbol{\pi} = U^\dagger \mathbf{p}, \quad \eta_{bk}^W = \sum_{\text{all } w}\sum_{i=1}^{h} \left(U_{ib}^{wW}\right)^* \tilde{r}_{ik}^w,$$
$$\pi_{bk}^W = \sum_{\text{all } w}\sum_{i=1}^{h} \left(U_{ib}^{wW}\right)^* p_{ik}^w, \quad \left[\eta_{qk}^W, \pi_{pk'}^{W'\dagger}\right] = ih\delta_{WW'}\delta_{qp}\delta_{kk'},$$
$$\boldsymbol{a}_b^W = \sqrt{\frac{m\omega_b^W}{2\hbar}}\left(\boldsymbol{\eta}_b^W + i\frac{\boldsymbol{\pi}_b^W}{m\omega_b^W}\right), \quad \left[a_{bk}^W, a_{dk'}^{W'\dagger}\right] = \delta_{WW'}\delta_{bd}\delta_{kk'}. \tag{22}$$

In analogy to the Hückel eigenstates $|Q, q)$, η_{bk}^W and π_{bk}^W are the components of the canonical position and momentum vectors of the vibrational problem and allow us to rewrite the vibrational Hamiltonian as

$$H_v = \sum_{\text{all } W}\sum_{b=1}^{h}\left(\frac{1}{2m}\boldsymbol{\pi}_b^{W\dagger}\boldsymbol{\pi}_b^W + \frac{1}{2}m\omega_b^2\boldsymbol{\eta}_b^{W\dagger}\boldsymbol{\eta}_b^W\right). \tag{23}$$

From their definitions, these coordinates are complex; however, if required, it is possible to construct real counterparts employing linear combinations of the pairs of canonical coordinates whose associated frequencies are degenerate. In our notation, $\boldsymbol{\eta}_h^{SS}$ is proportional to the center of mass of the molecule with $\omega_h^{SS} = 0$. Using (22), it is possible to

rewrite (23) as (11). In case we needed to consider anharmonicity and due to the fact that (23) is already separated by modes, we could replace the second term by the appropriate Morse potential [33,34]. For spectroscopic purposes, $\mathbf{p}_{\text{c.m.}} = 0$ is always chosen. Equation (22) allows us to interpret the vibrational excitations (relaxations) of the molecule as the production (absorption) of phonons propagating throughout the molecule; molecular recoil will be ignored.

It can be proved that the position vectors defined in (20) can be rewritten as

$$\tilde{\mathbf{r}}_i^w = \sum_{\text{all } W} \sum_{b=1}^{h} \sqrt{\frac{\hbar}{2m\omega_b}} \left[U_{ib}^{wW} \boldsymbol{a}_b^W + \left(U_{ib}^{wW}\right)^* \boldsymbol{a}_b^{W\dagger} \right] + \mathbf{r}_{\text{c.m.}}, \tag{24}$$

where terms $W = SS$ and $b = h$ are not included in the sum. It also holds that for nearest neighbors $\tilde{\mathbf{r}}_i^w - \tilde{\mathbf{r}}_j^{w'} = \mathbf{r}_{w',j}^{w,i}$.

III. INTERACTION HAMILTONIAN

The interaction Hamiltonian is the element of our model that supersedes the Born-Oppenheimer approximation, producing strong correlations between electrons and phonons, thus requiring the definition of dressed states for the solution of the whole system. We analyze these effects in the following.

A. Jaynes-Cummings treatment

We can rewrite (7) using the base of electronic modes $|W, q)$ and the annihilation and creation operators $\boldsymbol{a}_b^W$ and $\boldsymbol{a}_b^{W\dagger}$; it is convenient to introduce the chiral basis to rewrite the components in the $\hat{x}\hat{y}$ plane of the creation and annihilation operators:

$$a_{br}^W = \tfrac{1}{2}\left(a_{bx}^W + i a_{by}^W\right), \quad a_{bl}^W = \tfrac{1}{2}\left(a_{bx}^W - i a_{by}^W\right). \tag{25}$$

In this fashion, we obtain

$$H_i = \sum_{WQP} \sum_{b,q,p}^{h} \sum_{k}^{r,l,z} \left[\gamma_{qp}^{bk} \Lambda_{bk,qp}^{WQP} a_{bk}^W + \left(\gamma_{pq}^{bk} \Lambda_{bk,pq}^{WQP}\right)^* \left(a_{bk}^W\right)^\dagger \right] \sigma_{qp}^{QP}, \tag{26}$$

where W, Q, and P are symmetry labels. Furthermore, the following definitions are made:

$$\Lambda_{bk,qp}^{WQP} = -\frac{\Delta_0}{\lambda} \sqrt{\frac{\hbar}{32mh}} \sum_{c=1}^{5} \frac{A_{bk}^{Wc}}{\sqrt{\omega_b^W}} \left[B_{qp}^{QPc} + \left(B_{pq}^{QPc}\right)^* \right]. \tag{27}$$

The coefficients A_{bk}^{Wc} and B_{qp}^{QPc} are explained in Appendix A and the coefficients γ_{qp}^{bk} are defined as

$$\gamma_{qp}^{bz} = \delta_{b,q-p}, \quad \gamma_{qp}^{br} = \delta_{b,q-p+1}, \quad \gamma_{qp}^{bl} = \delta_{b,q-p-1}. \tag{28}$$

Analogously to what happens with the segment label (see Fig. 2), in case these coefficients demand that $q - p = b < 0$, we must instead take $b \bmod h$, which gives rise to the umklapp effect (details are given in Sec. III B 1). Now, as previously stated, we can use an analogous method for the construction of the Jaynes-Cummings model to find transition rates between electronic and vibrational modes by first introducing an interaction picture; the procedure is well known in the literature [35]. We infer that by taking the unperturbed Hamiltonian as

$$H_0 = H_e + H_v, \tag{29}$$

the interaction term in the interaction picture H_I acquires a time dependence of the form

$$H_I = \sum_{WQP} \sum_{b,q,p}^{h} \sum_{k}^{r,l,z} \left[\gamma_{qp}^{bk} \Lambda_{bk,qp}^{WQP} a_{bk}^W e^{i(-\omega_b + \nu_q - \nu_p)t} + \left(\gamma_{pq}^{bk} \Lambda_{bk,pq}^{WQP}\right)^* \left(a_{bk}^W\right)^\dagger e^{i(\omega_b + \nu_q - \nu_p)t} \right] \sigma_{qp}^{QP}. \tag{30}$$

This function provides the transition amplitudes via the integral

$$c(t) = -\frac{i}{\hbar} \int_{t_0}^{t} dt' \langle f | H_I(t') | i \rangle. \tag{31}$$

In this expression it is assumed that the precise state of the molecule is known at $t = t_0$. The interaction term (30) is the same as in the usual sudden application of a perturbative field; however, it is not really applied to a stationary system. Instead, the initial state is already chosen as a direct product of electronic and vibrational degrees of freedom and evolves according to the full Hamiltonian. The transition rates tend to be more pronounced for those between states of similar energy, in other words, transitions whose Bohr frequencies are close to zero,

$$\omega_{b(q,p)}^W - \left|\nu_q^Q - \nu_p^P\right| \approx 0, \tag{32}$$

where we consider that the index b can be written in terms of indices p and q based on (28). Here we note that since we exclude the motion of the molecule's center of mass, we always have $\omega_b^W \neq 0$; thus we require electronic transitions such that $|\nu_q^Q - \nu_p^P| \neq 0$ (the degenerate states are automatically excluded). Now, as in the case of the Jaynes-Cummings model, we take this idea one step further and implement the rotating-wave approximation, which is equivalent to the use of an infinite upper integration limit in (31) and the disregard of all the terms that do not satisfy the condition (32) in favor of the few that do satisfy it.

The mathematical restrictions (28) and (32) over the Bloch momenta and the selection rules implicit in (27) are all independent of each another. A detailed analysis is now provided.

B. Selection rules

Although all possible combinations of electron-phonon couplings are present in the interaction Hamiltonian (26), there exist various selection rules that restrict the actual number of available couplings in the dynamics; such restrictions are based on symmetry and conservation laws. The former occurs in a manner analogous to the Laporte rule in electric dipole transitions and the latter is addressed in the following.

1. Conservation of Bloch's momentum and conservation of energy

The first selection rule that emerged in the system is manifested in coefficients (28), which set a restriction for the Bloch momentum of the vibrational normal modes and Hückel eigenstates. When an electronic transition takes place, the electronic Bloch wave propagated through the molecule

suffers a change in wavelength, which is allowed if the difference in momentum $\hbar b/\lambda = \hbar(q-p)/\lambda$ is transmitted or absorbed from the vibrational wave. In Fig. 1 we show a representation of this process; the Hückel eigenstates are depicted with probability densities, while the vibrational mode is represented with a deformation of the molecule.

From γ_{qp}^{bz} it is evident that the Bloch momentum b of the vibrational wave compensates for the transition from the electronic state with Bloch momentum p to the electronic state with Bloch momentum q. Note that if $q < p$, we would require b to be negative, which would take it outside the analogous Brillouin zone (ranging over the natural numbers from 1 to h). Thus a multiple of h has to be added in order to keep $b > 0$; from their definition, none of these indices can be negative. We recognize this occurrence as a manifestation of the umklapp scattering in a discrete medium.

For vibrations on the $\hat{z}$ axis (transverse elastic waves) the Bloch wave is orthogonal to the direction of its propagation. This is not the case for waves in the $\hat{x}\hat{y}$ plane (which contain longitudinal polarization). For this reason we lack an optical equivalent for this kind of in-plane propagation. In order for the in-plane waves to complete a cycle, they must bend from site to site according to the structure of the molecule; as a result, they either gain or lose an additional quantum of angular momentum in each cycle, depending on the chirality of the wave (left or right). The Bloch momentum conservation must account for this effect in the polarization of the in-plane vibrational waves, which is observed in γ_{qp}^{br} and γ_{qp}^{bl} in (28) above.

2. Permutation symmetry

As previously stated, from Fig. 2(a) we can infer that the system is invariant under parity on the $\hat{z}$ axis or, equivalently, under the permutation of the upper and lower chains $\hat{\pi}$, we can deduce all the effects that this transformation has over all the components of the molecule:

$$\hat{\pi}^2 = 1, \quad \hat{\pi}H_e\hat{\pi} = H_e, \quad \hat{\pi}H_v\hat{\pi} = H_v, \quad \hat{\pi}H_i\hat{\pi} = H_i, \quad \hat{\pi}\tilde{\mathbf{r}}_{11i}\hat{\pi} = \tilde{\mathbf{r}}_{21i}, \quad \hat{\pi}\tilde{\mathbf{r}}_{12i}\hat{\pi} = \tilde{\mathbf{r}}_{22i}, \quad \hat{\pi}\,|11i\rangle = |21i\rangle\,,$$
$$\hat{\pi}\,|12i\rangle = |22i\rangle\,, \quad \hat{\pi}\hat{\mathbf{R}}_{11i}^{12i}\hat{\pi}\cdot\hat{z} = -\hat{\mathbf{R}}_{11i}^{12i}\cdot\hat{z}, \quad \hat{\pi}\hat{\mathbf{R}}_{21i}^{11i}\hat{\pi} = -\hat{\mathbf{R}}_{21i}^{11i}, \quad \hat{\pi}\hat{\mathbf{R}}_{11i}^{12i}\hat{\pi}\cdot\hat{x} = \hat{\mathbf{R}}_{11i}^{12i}\cdot\hat{x}, \quad \hat{\pi}\hat{\mathbf{R}}_{11i}^{12i}\hat{\pi}\cdot\hat{y} = \hat{\mathbf{R}}_{11i}^{12i}\cdot\hat{y}. \tag{33}$$

Along with the effects of $\hat{\pi}_s$, these relations were used for the labeling of electronic and vibrational normal modes in Secs. II C 1 and II C 2. The operator $\hat{\pi}$ thus changes the atomic position vectors, the (orbital) site kets, and the equilibrium position vectors on the $\hat{z}$ axis. Evidently, after implementing the change of bases, these modifications are reflected, respectively, in the creation and annihilation operators, the Hückel eigenstates, and coefficients R_z (defined in Appendix A), explicitly,

$$\hat{\pi}\boldsymbol{a}_b^{SS}\hat{\pi} = \boldsymbol{a}_b^{SS}, \quad \hat{\pi}\boldsymbol{a}_b^{SA}\hat{\pi} = \boldsymbol{a}_b^{SA}, \quad \hat{\pi}\boldsymbol{a}_b^{AS}\hat{\pi} = -\boldsymbol{a}_b^{AS}, \quad \hat{\pi}\boldsymbol{a}_b^{AA}\hat{\pi} = -\boldsymbol{a}_b^{AA}, \quad \hat{\pi}\,|SS,q\rangle = |SS,q\rangle, \quad \hat{\pi}\,|SA,q\rangle = |SA,q\rangle,$$
$$\hat{\pi}\,|AS,q\rangle = -|AS,q\rangle, \quad \hat{\pi}\,|AA,q\rangle = -|AA,q\rangle, \quad \hat{\pi}R_z^c\hat{\pi} = -R_z^c, \quad \hat{\pi}R_{xy}^c\hat{\pi} = R_{xy}^c, \quad c = 1,2,3,4,5. \tag{34}$$

We may now rewrite (30) as

$$H_i = \sum_{WQP}\sum_{b,q,p}^{h}\sum_{k}^{r,l,z}\sum_{c=1}^{5} C_{bk,qp}^{Wc,QP} H_{bk,qp}^{Wc,QP} + \text{H.c.},$$
$$H_{bk,qp}^{Wc,QP} = R_k^c a_{bk}^W \sigma_{qp}^{QP}, \tag{35}$$

where the sum is carried over all indices and $C_{bk,qp}^{Wc,QP}$ encapsulates all the coefficients defined so far. Since H_i must remain invariant under permutation of the upper and lower chains, only the couplings that leave the overall sign untouched are allowed; to achieve this, the three elements of each term $H_{bk,qp}^{Wc,QP}$ must coordinate to have an even number of sign changes. In Table I we show all possible couplings and whether they are allowed in the dynamics (✓) or not (✗); the same rules apply for terms containing creation operators. We note that the selection rule is reversed on the $\hat{z}$ axis compared to the $\hat{x}\hat{y}$ plane.

TABLE I. Couplings between electronic transitions σ and phononic excitations a on the $\hat{z}$ axis and $\hat{x}\hat{y}$ plane that are consistent with the permutation symmetry (33).

$R_z(R_{xy})$	a_b^{SS}, a_b^{SA}	a_b^{AS}, a_b^{AA}
$\sigma_{qp}^{SS,SS}, \sigma_{qp}^{SA,SA}, \sigma_{qp}^{AS,AS}, \sigma_{qp}^{AA,AA}$	✗(✓)	✓(✗)
$\sigma_{qp}^{AS,SS}, \sigma_{qp}^{AA,SA}, \sigma_{qp}^{SA,AS}$	✓(✗)	✗(✓)

This is due to the fact that the overall vibrational wave has a different parity when the individual molecular sites vibrate with the same periodicity but in different directions. In Fig. 5 we see some examples of this effect: The third symbol on the left adjusts the symmetry of the first symbol at the center, e.g.,

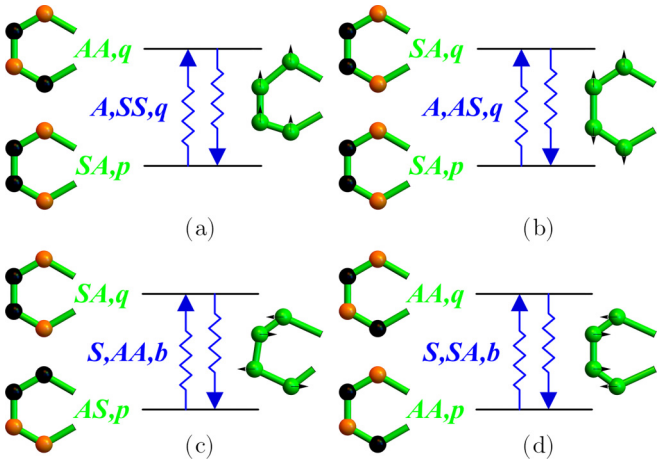

FIG. 5. Symmetry of electronic transitions mediated by a phonon. Oscillations are represented on (a) and (b) the $\hat{z}$ axis and (c) and (d) the $\hat{x}\hat{y}$ plane. The upper and lower chains oscillate in synchrony in (a) and (c), while in (b) and (d) the oscillation is mirrored.

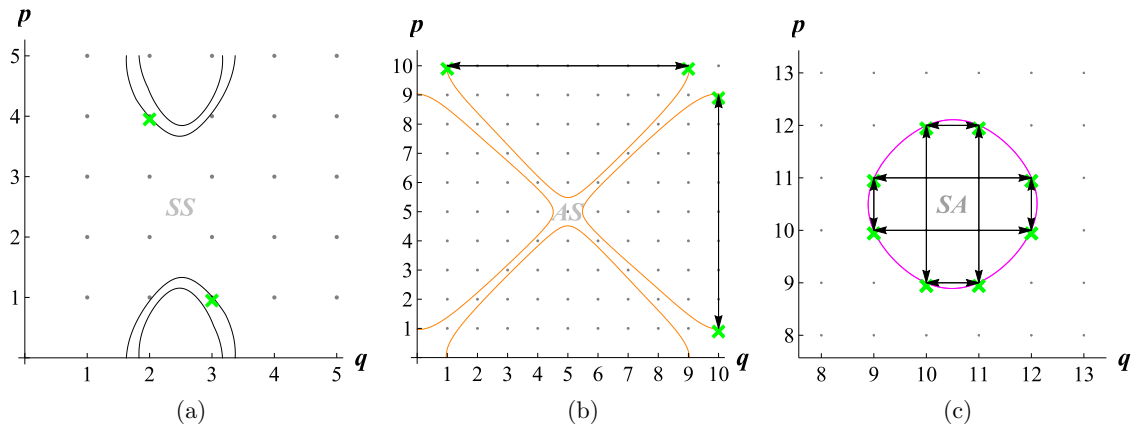

FIG. 6. Examples of level curves originated from the conservation of energy and Bloch momentum (solutions represented by crosses). (a) Two electron-phonon systems of two levels in a [5]cycloacene molecule. (b) Three-level electronic system in a [10]cycloacene molecule. (c) Magnified region of viable solutions for [21]cycloacene.

the label A, SS indicates all four carbon atom in each benzene vibrate in synchrony; however, since it happens on the $\hat{z}$ axis, the overall symmetry of the oscillation is antisymmetric.

C. Physical realizations

From the expressions (17) and (21) and after introducing the known parameters (obtained from spectroscopy experiments [29,30,36])

$$|\Delta_0| = 2.7\ \text{eV}, \quad \sqrt{k/m} = 3.94 \times 10^{14}\ \text{Hz},$$
$$|\Delta_0|/(\hbar\sqrt{k/m}) \approx 0.096, \tag{36}$$

we can deduce all the possible couplings inside the molecule by first interpreting indices q and p as continuum variables; thus the restriction (32) becomes a transcendental equation. By inspection of Fig. 3, we note that $|\nu_q^Q - \nu_p^P|$ generates five different expressions, but only three of them lead to quantities that have the same order of magnitude as the four vibrational bands $\omega^W_{b(q,p)}$; thus the total number of relevant level curves is 12. We note that since many pairs of energy levels have the same separation, a given level curve may explain more than one electronic transition. In order to find the plausible electron-phonon couplings, we only have to overlay the point lattice spanned by q and p and recognize all the points that overlap approximately with the level curves (see the crosses in Fig. 6). In our procedure, h is the only free parameter which allows us to study the presence of simplified vibronic-electronic couplings as functions of the size. One last thing to discuss is the fact that due to the discrete nature of the indices, it is unlikely that we will obtain an exact zero from the subtraction in (32), which demands a factor of tolerance. The simplest answer is to take only the transitions that lead to differences below the lowest vibrational normal frequency, which depends on h; therefore we define

$$\mathscr{O}_h = \frac{\hbar\sqrt{k/m}}{\Delta_0}\sqrt{2 - 2\cos\left(\frac{\pi}{h}\right)} \tag{37}$$

as the maximum tolerance for an effective zero. In this manner, we give a precise numerical margin for (32),

$$\mathscr{O}^{WQP}_{bqp}(h) = \left(\omega^W_{b(q,p)} - \left|\nu_q^Q - \nu_p^P\right|\right)/\mathscr{O}_h < \tfrac{1}{4}, \tag{38}$$

where we choose a fourth of the maximum tolerance to make it half the zero-point energy of phonons, which follows from (11).

In Figs. 6(a)–6(c) we show three examples of the level curves that can be obtained for transverse elastic waves. The abscissa (ordinate) indicates the Bloch momentum of the initial (final) state. The gray dots are the lattice of points truly spanned by (q, p) [the Bloch momenta of states $|Q, q)$ and $|P, p)$, respectively] and the crosses highlight the couplings found in each case; only these dots satisfy the established tolerance (38). The pair of symbols at the center indicates the symmetry of the vibrational mode mediating the electronic transition. Finally, the black arrows indicate that the electronic state with Bloch momentum $q(p)$ can transit to more than one final state, giving rise to a multilevel system.

D. Multilevel systems on the $\hat{z}$ axis

Once we have factored in all the selection rules, we may study an arbitrary multilevel system under the approximation of conserved excitations. First, we note that since the restrictions (32) and (38) are invariant under $q \to h - q$ and $p \to h - p$, we always encounter an even pair of couplings, regardless of the number of benzene rings in the molecule.

1. Two-level system ($\hat{z}$ axis)

Each cross present in Figs. 6(a)–6(c) is indicative that an electronic transition σ^{QP}_{qp} such that $\nu_q^Q - \nu_p^P > 0$ is coupled to the annihilation of the phonon a^W_b. If instead we have $\nu_q^Q - \nu_p^P < 0$, the coupling occurs with the creation of such a phonon $a^{W\dagger}_b$. In Fig. 6(a) we show the simplest possible coupling. We note that both transitions between the bands $\nu^{SS} \leftrightarrow \nu^{AS}$ and $\nu^{AA} \leftrightarrow \nu^{SA}$ lead to the same numeric tolerance and since the level curve includes crosses (for the reason stated in Sec. III D), we have a total of four transitions and the corresponding interaction Hamiltonian is

$$H_I = \Lambda^{W,AS,SS}_{bz,pq} a^W_{bz}\sigma^{AS,SS}_{pq} + \left(\Lambda^{W,AS,SS}_{bz,pq}\right)^* \left(a^W_{bz}\right)^\dagger \sigma^{AS,SS}_{qp}$$
$$+ \Lambda^{W,AS,SS}_{\bar{bz},\bar{p}\bar{q}} a^W_{\bar{bz}}\sigma^{AS,SS}_{\bar{p}\bar{q}} + \left(\Lambda^{W,AS,SS}_{\bar{bz},\bar{p}\bar{q}}\right)^* \left(a^W_{\bar{bz}}\right)^\dagger \sigma^{AS,SS}_{\bar{q}\bar{p}}$$

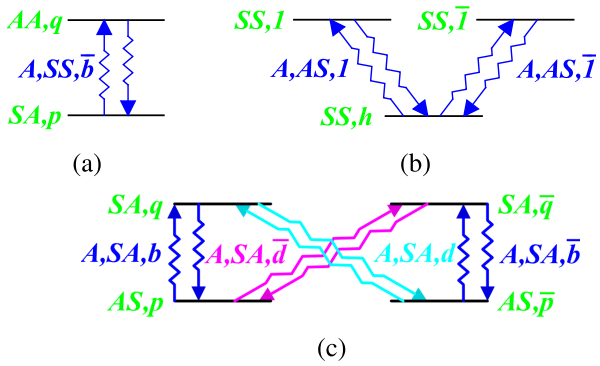

FIG. 7. Phonon-assisted transition diagrams for two-, three-, and four-level systems and their parity rules. (a) Two-level system. (b) Three-level system with twofold degeneracy. (c) Four-level system with two doublets. The symmetry labels are explained in Fig. 5

$$+\Lambda^{W,AA,SA}_{\bar{b}z,qp}a^{W}_{\bar{b}z}\sigma^{AA,SA}_{qp}+\left(\Lambda^{W,AA,SA}_{\bar{b}z,qp}\right)^{*}\left(a^{W}_{\bar{b}z}\right)^{\dagger}\sigma^{AA,SA}_{pq}$$
$$+\Lambda^{W,AA,SA}_{bz,\bar{q}\bar{p}}a^{W}_{bz}\sigma^{AA,SA}_{\bar{q}\bar{p}}+\left(\Lambda^{W,AA,SA}_{bz,\bar{q}\bar{p}}\right)^{*}\left(a^{W}_{bz}\right)^{\dagger}\sigma^{AA,SA}_{\bar{p}\bar{q}}, \tag{39}$$

where $\bar{b}:=h-b$ and $\bar{q}:=h-q$. This formula applies for both $W=SS,SA$. In particular, $W=SS$ is illustrated in Fig. 7(a). We note that from (21) we can guarantee that $\omega_b=\omega_{\bar{b}}$; this can also be inferred from Fig. 4. Furthermore, we can prove that $|\Lambda^{WQP}_{bz,pq}|=|\Lambda^{WQP}_{\bar{b}z,\bar{p}\bar{q}}|$ (note that if $d=\bar{b}$, then $\bar{d}=b$); therefore we can write (39) in the following way:

$$H_I=|\Lambda'|(a\sigma'_{+}+a^{\dagger}\sigma'_{-}+b\tau'_{+}+b^{\dagger}\tau'_{-})$$
$$+|\Lambda|(a\sigma_{+}+a^{\dagger}\sigma_{-}+b\tau_{+}+b^{\dagger}\tau_{-}). \tag{40}$$

In this expression, $\sigma_{\pm},\tau_{\pm},\sigma'_{\pm},\tau'_{\pm}$ operate on different electronic states such that each line in (40) is identical to two uncoupled Jaynes-Cummings Hamiltonians, explicitly,

$$H_{\mathrm{JC2}}=a\sigma_{+}+a^{\dagger}\sigma_{-}. \tag{41}$$

The system described by this expression is illustrated in Fig. 7(a), where we see that there are only two states upon which this operator can act. Moreover, the vibrational phonon (zigzag arrow) mediates the transition between the electronic levels (horizontal lines) and the symbol A in A,SS indicates that the transition occurs for transverse waves ($\hat{z}$ axis). The latter is antisymmetric under the parity operation (33). We infer

$$H_{\mathrm{JC2}}|gn]=\sqrt{n}|e,n-1],\quad H_{\mathrm{JC2}}|e,n-1]=\sqrt{n}|gn],$$
$$|gn]=|SA,p)\left|n^{SS}_{bz}\right\rangle,$$
$$|e,n-1]=(\Lambda/|\Lambda|)|AA,q)\left|(n-1)^{SS}_{bz}\right\rangle, \tag{42}$$

where $|n^{W}_{bz}\rangle$ is the occupation state corresponding to creation and annihilation operators (22). It is well known that solutions to this type of systems are given in terms of dressed states,

$$|K_2\varepsilon]=\frac{1}{\sqrt{2}}(|e,n-1]+\varepsilon|gn]),\quad H_{\mathrm{JC2}}|K_2\varepsilon]=\varepsilon\sqrt{K_2/2}|K_2\varepsilon],$$
$$K_2=2n,\ \varepsilon=-1,1, \tag{43}$$

with the exception $H_{\mathrm{JC2}}|g0]=0$. It is noteworthy that the infinite set of states $|gn]$, $|e,n-1]$ can be divided into sets of 2×2 representations. This is due to the following conserved quantity, i.e., an operator that commutes with H_I:

$$\hat{K}_2=2a^{\dagger}a+\sigma_z+1,\quad \sigma_z=[\sigma_{+},\sigma_{-}],$$
$$\hat{K}_2|gn]=K_2|gn],\quad \hat{K}_2|e,n-1]=K_2|e,n-1]. \tag{44}$$

It should be mentioned that the phonon in the first (second) line of (39) appears again in the fourth (third) line; therefore, the algebraic description is the same as a Tavis-Cummings model in which two two-level electronic systems are coupled to the same bosonic mode.

Each cross is indicative of one term of the type (41). This is true for all transitions; however, not all of them lead to two-level systems.

2. *Three-level system ($\hat{z}$ axis)*

In Fig. 6(b) we show an example of an electronic state with Bloch momentum h that can transit to either of the states with Bloch momenta 1 and $h-1$, meaning that we have a three-level system. Note that although we have four crosses, in this case, two of them are reiterations; this happens due to the fact that this is an intraband transition and indices q and p are interchangeable in this case only. This is true for transitions between the bands $\nu^{SS}\leftrightarrow\nu^{SS}$, $\nu^{SA}\leftrightarrow\nu^{SA}$, $\nu^{AS}\leftrightarrow\nu^{AS}$, and $\nu^{AA}\leftrightarrow\nu^{AA}$. In Sec. III D 1 we included all the possibilities; here we will only focus on the $\nu^{SS}\leftrightarrow\nu^{SS}$ case, which is illustrated in Fig. 7(b). The interaction Hamiltonian in this case is

$$H_I=\Lambda^{W,SS,SS}_{1z,1,h}a^{W}_{1z}\sigma^{SS,SS}_{1,h}+\left(\Lambda^{W,SS,SS}_{1z,1,h}\right)^{*}a^{W\,\dagger}_{1z}\sigma^{SS,SS}_{h,1}$$
$$+\Lambda^{W,SS,SS}_{\bar{1}z,\bar{1},h}a^{W}_{\bar{1}z,\bar{1}}\sigma^{SS,SS}_{\bar{1},h}+\left(\Lambda^{W,SS,SS}_{\bar{1}z,\bar{1},h}\right)^{*}a^{W\,\dagger}_{\bar{1}z,\bar{1}}\sigma^{SS,SS}_{h,\bar{1}}, \tag{45}$$

where $W=AS,AA$ are both possible. We abbreviate (45) in the following manner:

$$H_I=|\Lambda|H_{\mathrm{JC3}},$$
$$H_{\mathrm{JC3}}=a\sigma_{+}+a^{\dagger}\sigma_{-}+b\tau_{+}+b^{\dagger}\tau_{-}. \tag{46}$$

This expression is similar to (40); this time, however, $\sigma_{\pm}$ and $\tau_{\pm}$ share the same lower state, which can be appreciated in Fig. 7(b). We note that the phonons mediating each electronic transition are different. As a result, H_{JC3} is now diagonalized in 3×3 blocks. To see that we first note that

$$H_{\mathrm{JC3}}|gn_an_b]=\sqrt{n_a}|e,n_a-1,n_b]+\sqrt{n_b}|\bar{e}n_a,n_b-1],\quad H_{\mathrm{JC3}}|en_a-1,n_b]=\sqrt{n_a}|gn_an_b],$$
$$H_{\mathrm{JC3}}|\bar{e}n_a,n_b-1]=\sqrt{n_b}|gn_an_b],\quad |gn_an_b]=(\Lambda^{*}/|\Lambda|)|SS,h)\left|n^{W}_{bz}\right\rangle\left|n^{W}_{\bar{b}z}\right\rangle,$$
$$|e,n_a-1,n_b]=|SS,1)\left|(n-1)^{W}_{bz}\right\rangle\left|n^{W}_{\bar{b}z}\right\rangle,\quad |\bar{e}n_a,n_b-1]=|SS,\bar{1})\left|n^{W}_{bz}\right\rangle\left|(n-1)^{W}_{\bar{b}z}\right\rangle. \tag{47}$$

These relations allow us to derive the eigenstates of the coupled system:

$$|K_3 k0] = \sqrt{\frac{n_b}{n_a+n_b}}|e, n_a-1, n_b] - \sqrt{\frac{n_a}{n_a+n_b}}|\bar{e}n_a, n_b-1],$$
$$|K_3 k, \pm 1] = \pm\frac{1}{\sqrt{2}}|gn_a n_b] + \sqrt{\frac{n_a}{2(n_a+n_b)}}|e, n_a-1, n_b] + \sqrt{\frac{n_b}{2(n_a+n_b)}}|\bar{e}n_a, n_b-1],$$
$$K_3 = 3(n_a+n_b),\ k = n_a - n_b,\quad k = -K_3/3, -K_3/3+2, \ldots, K_3/3-2, K_3/3,\quad H_{\mathrm{JC3}}|K_3 k\varepsilon] = \varepsilon\sqrt{K_3/3}|K_3 k\varepsilon],$$
$$\varepsilon = -1, 0, 1. \tag{48}$$

If either $n_a = 0$ or $n_b = 0$, these solutions reduce to a two-level system in accordance with (43). Once again we have found finite representations from an infinite set of states. In contrast with the two-level case, now we have two occupation numbers $n_a = 0, 1, 2, \ldots$ and $n_b = 0, 1, 2, \ldots$, hence the requirement of the conserved quantities K_3 and k, originated from the following operators:

$$\hat{K}_3 = 3(a^\dagger a + b^\dagger b) + \sigma_z + \tau_z + 2,\quad \hat{k} = a^\dagger a - b^\dagger b + \sigma_z - \tau_z,\quad \tau_z = [\tau_+, \tau_-],\quad \hat{K}_3|K_3 k\varepsilon] = K_3|K_3 k\varepsilon],\quad \hat{k}|K_3 k\varepsilon] = k|K_3 k\varepsilon]. \tag{49}$$

Not only are the results for the transitions between the bands $\nu^{SA} \leftrightarrow \nu^{SA}$, $\nu^{AS} \leftrightarrow \nu^{AS}$, and $\nu^{AA} \leftrightarrow \nu^{AA}$ analogous to (49), but the phonons mediating their energy eigenstates are the same. This allows us to draw another parallel to a Tavis-Cummings model, but with a three-level electronic system. In this context we have the occurrence of the following phenomenon.

3. Peierls distortion

The eigenstates of the three-electronic-level system (48) are also eigenstates of the unperturbed Hamiltonian (29) with the same eigenvalue:

$$H_0|K_3 k\varepsilon] = \left[\hbar\nu_h^{SS} + \hbar\omega_1^W(n_a+n_b)\right]|K_3 k\varepsilon]. \tag{50}$$

For the sake of clarity, the energy contribution from the remaining occupation numbers and the vibrational rest energy were omitted. This is due to the fact that $\nu_1^{SS} = \nu_{\bar{1}}^{SS}$ and $\omega_1^W = \omega_{\bar{1}}^W$ and due to the condition of conservation of energy (32). These eigenvalues are the energies of the uncoupled problem and are simply the sum of both degrees of freedom. However, the complete Hamiltonian requires the corrections made by H_I, thus generating an adjustment to the energy eigenvalue of the full system. In particular, we are interested in the eigenvalue of $|K_3 k, -1]$:

$$H|K_3 k, -1] = E|K_3 k, -1],$$
$$E = \left[\hbar\nu_h^{SS} + \hbar\omega_1^W(n_a+n_b) - |\Lambda|\sqrt{n_a+n_b}\right]. \tag{51}$$

This dressed state is able to produce an energy below the ground state of the unperturbed Hamiltonian (which is $\hbar\nu_h^{SS}$), which generates a Peierls distortion where the state of minimal energy of the complete system includes an excited vibrational state. In Fig. 8 we see how the energy eigenvalue varies as a function of the ratio $\hbar\omega/|\Lambda|$ and we note that at $K_3 = 0$ we have the unperturbed system. We also note that at $x \approx 0$ the energies are below the unperturbed ground state, as expected (Peierls distortion), and at $x \gg 0$ the separation in energy levels tends to the usual harmonic behavior. The suggested values of molecular parameters considered in Sec. III C do not lead to a distortion of this kind. In order to achieve it, we need to either reduce the vibrational amplitude $\sqrt{k/m}$ or increase the electronic coupling Δ_0.

4. Four-level systems ($\hat{z}$ axis)

In full similarity to the systems presented so far, each black rectangle of Fig. 6(c) illustrates a scenario in which the electron can transit through four different states (here we analyze only one of the rectangles, since the description is the same for both). It is remarkable that this coupling can only occur between the $\nu^{SA} \leftrightarrow \nu^{AS}$ electronic bands, which points to a realization of a Jaynes-Cummings model generalized to four levels. The corresponding interaction Hamiltonian is

$$\begin{aligned} H_I = {} & \Lambda^{SA,SA,AS}_{bz,qp} a^{SA}_{bz} \sigma^{SA,AS}_{qp} + \left(\Lambda^{SA,SA,AS}_{bz,qp}\right)^* a^{SA\,\dagger}_{bz} \sigma^{AS,SA}_{pq} \\ & + \Lambda^{SA,SA,AS}_{\bar{b}z,\bar{q}\bar{p}} a^{SA}_{\bar{b}z} \sigma^{SA,AS}_{\bar{q}\bar{p}} + \left(\Lambda^{SA,SA,AS}_{\bar{b}z,\bar{q}\bar{p}}\right)^* a^{SA\,\dagger}_{\bar{b}z} \sigma^{AS,SA}_{\bar{p}\bar{q}} \\ & + \Lambda^{SA,SA,AS}_{dz,q\bar{p}} a^{SA}_{dz} \sigma^{SA,AS}_{q\bar{p}} + \left(\Lambda^{SA,SA,AS}_{dz,q\bar{p}}\right)^* a^{SA\,\dagger}_{dz} \sigma^{AS,SA}_{\bar{p}q} \\ & + \Lambda^{SA,SA,AS}_{\bar{d}z,\bar{q}p} a^{SA}_{\bar{d}z} \sigma^{SA,AS}_{\bar{q}p} + \left(\Lambda^{SA,SA,AS}_{\bar{d}z,\bar{q}p}\right)^* a^{SA\,\dagger}_{\bar{d}z} \sigma^{AS,SA}_{p\bar{q}}, \end{aligned} \tag{52}$$

which can be written as

$$\begin{aligned} H_I = {} & |\Lambda|(a\sigma_+ + a^\dagger\sigma_- + b\tau + b^\dagger\tau_-) \\ & + |\bar{\Lambda}|(\bar{a}\bar{\sigma}_+ + \bar{a}^\dagger\bar{\sigma}_- + \bar{b}\bar{\tau} + \bar{b}^\dagger\bar{\tau}_-). \end{aligned} \tag{53}$$

Unlike the previous cases, this coupling can only occur with the $W = SA$ symmetry. Although the algebraic description is similar to the two- and three-level systems, the degeneracy

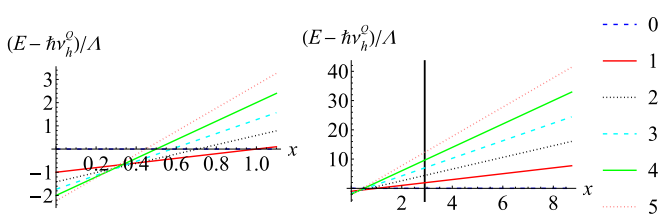

FIG. 8. Energy eigenvalue (51) as a function of $x = \hbar\omega/|\Lambda|$ in dimensionless units. Each line represents a different value of $K_3/3$. The black vertical line indicates the point ($x = 2.9$) that coincides with the parameters implemented in (36) and Fig. 6(b).

changes the nature of the couplings, and from Fig. 7(c) we infer that this system is more complex than the aforementioned two. It is possible to find a conserved quantity by first defining the operator

$$K_4 = 4(a^\dagger a + b^\dagger b + \bar{a}^\dagger \bar{a} + \bar{b}^\dagger \bar{b}) + \sigma_z + \tau_z + \bar{\sigma}_z + \bar{\tau}_z, \tag{54}$$

which divides the system into blocks where the sum of active phonons is conserved; further reductions are beyond the scope of the present work.

IV. CONCLUSION

We have successfully developed an algebraic model of the cycloacene molecule that couples its internal degrees of freedom, allowing deformations beyond the Born-Oppenheimer approximation. Due to the symmetry of the molecule, we were able to define a phononic basis to study its vibrations in a fashion similar to media with discrete symmetry such as graphene [37]. Moreover, we also found phenomena commonly associated with these systems such as the umklapp effect in the conservation of Bloch momentum. A connection to models of atoms inside an electromagnetic cavity was made as well, since the process in which the electronic transitions may occur is described in an analogous manner to the Jaynes-Cummings model, which is algebraically solvable.

As expected from a molecule rich in symmetry, the electronic transitions were limited by selection rules that included parity invariance, conservation of energy, and conservation of the total Bloch momentum. From these rules a criterion similar to the Laporte rule was obtained and a collection of level curves that describe the possible solutions in the parameter space was found.

Regarding our methods, most of the vibrational spectroscopy of a chemical compound, leaving aside their plasticity limit (Morse oscillators), can be described by adjacency matrices that share the system's symmetry under discrete operations. It is to be expected that universal shapes have similar spectroscopy in other physical realizations such as elastic systems, successfully demonstrated in recent works [38]. Although elastic vibrations of a material have been employed as both a realization of localized electronic orbitals and true vibrations of a compound, the physical-chemical counterpart also demands an interaction between these; while not directly evident in vibrational emulations of metallic structures, the decay laws governed by symmetry should be present as well in macroscopic systems subjected to perturbations (Fermi's golden rule).

Since we provided the complete spectrum of the molecule, by resorting to thermodynamical equilibrium, it is possible to obtain the probability distribution of all energy transitions as a function of temperature. This can prove beneficial in applications to quantum computing, where it is desirable to have a transition probability that favors a particular block of the Hamiltonian. Proposals of this type have been considered in the past [39].

It is noteworthy that a recurrent phenomenon in lattice systems such as Peierls distortion was found (with a polygonal symmetry in our case instead of the linear molecule). This implies that the ground state of the whole structure exhibits vibrational modes.

Since our results include excitations of phonons due to electronic transitions, they could be utilized to analyze luminescence in thermodynamic equilibrium. Moreover, given the structural analogy with other ring polymers, it is expected that the absorption spectrum of small cycloacene molecules is highly sensitive to the total number of segments within the system; this property has already been reported for methylene-bridged [*n*]cycloparaphenylenes [7].

ACKNOWLEDGMENTS

Financial support from CONAHCYT under Grant No. CF-2023-G-763 is acknowledged. R.A.M.S. was supported by DGAPA-UNAM under Project PAPIIT No. IN111021.

APPENDIX A: EXPLICIT INDEX NOTATION

In Sec. II we mentioned that there are five nearest neighbors in each benzene ring, following the direction of the arrows in Fig. 2(c). We define

$$\begin{aligned} &w_2(1) = 12, \quad w_2(2) = 11, \quad w_2(3) = 22, \quad w_2(4) = 21, \quad w_2(5) = 11, \quad w_1(1) = 11, \quad w_1(2) = 12, \quad w_1(3) = 21, \\ &w_1(4) = 22, \quad w_1(5) = 21, \quad I(1,i) = I(3,i) = I(4,i) = I(5,i) = i, \quad I(2,i) = i+1, \\ &J(1,i) = J(2,i) = J(4,i) = J(5,i) = i, \quad J(3,i) = i+1, \end{aligned} \tag{A1}$$

where $I(c,i)$ and $w_2(c)$ mark the final end of the arrows while $J(c,i)$ and $w_1(c)$ mark their beginning. We can now write the Hamiltonians (6), (7), and (8) as

$$H_e = \Delta_0 \left(\sum_{c=1}^{5} \sum_{i=1}^{h} |w_2(c), I(c,i)\rangle \langle w_1(c), J(c,i)| + \text{H.c.} \right), \tag{A2}$$

$$H_i = -\frac{1}{\lambda} \Delta_0 \sum_{c=1}^{5} \sum_{i=1}^{h} \left(\hat{\mathbf{R}}^{w_2(c),I(c,i)}_{w_1(c),J(c,i)} \right)^T \left(\mathbf{r}^{w_2(c),I(c,i)}_{w_1(c),J(c,i)} \right) |w_2(c), I(c,i)\rangle \langle w_1(c), J(c,i)| + \text{H.c.}, \tag{A3}$$

$$V_{\text{har}} = \frac{1}{2} k \sum_{c=1}^{5} \sum_{i=1}^{h} \left(\mathbf{r}^{w_2(c),I(c,i)}_{w_1(c),J(c,i)} \right)^2, \tag{A4}$$

respectively. We can also write the coefficients A_{bk}^{Wc} and B_{qp}^{QPc} explicitly:

$$A_{bk}^{Wc} = R_k^c A_b^{Wc}, \quad R_z^5 = \hat{\mathbf{R}}_{21i}^{11i}\cdot\hat{z} = 1\,\forall\, i, \quad R_z^1 = R_z^4 = -R_z^2 = -R_z^3 = \hat{\mathbf{R}}_{11i}^{12i}\cdot\hat{z} = \tfrac{1}{2}\,\forall\, i, \quad R_r^c = R_l^c = R_{xy}^c,$$
$$R_{xy}^5 = \hat{\mathbf{R}}_{21i}^{11i}\cdot\hat{x} = 0\,\forall\, i, \quad R_{xy}^1 = R_{xy}^2 = -R_{xy}^3 = -R_{xy}^4 = \hat{\mathbf{R}}_{11h}^{12h}\cdot\hat{x} = \sqrt{3}/2, \quad A_b^{Wc} = 2\sqrt{h}\big(U_{i(c),b}^{w_2(c),W} - U_{j(c),b}^{w_1(c),W}\big),$$
$$B_b^{QPc} = 2h\big(V_{i(c),q}^{w_2(c),Q}\big)^* V_{j(c),p}^{w_1(c),P}, \quad i(1) = i(3) = i(4) = i(5) = h, \quad i(2) = 1, \quad j(1) = j(2) = j(4) = j(5) = h, \quad j(3) = 1. \tag{A5}$$

APPENDIX B: EXPANSION OF THE COUPLING INTEGRALS

Here we present our evaluation of the couplings $\langle w, i|H_E|w', j\rangle$ introduced in (3). Recalling that we are studying the dynamics of a single electron throughout the delocalized π orbitals, we begin by writing a general expression of the electronic Hamiltonian H_E:

$$H_E = \frac{\mathbf{p}^2}{2m} - \sum_{\text{all } w}\sum_{i=1}^{h}\frac{Z_{\text{eff}}e^2}{|\mathbf{r}-\mathbf{r}_i^w|}. \tag{B1}$$

Since we are working with a tight-binding model, we make the analysis considering only a neighboring pair in the sum over atomic sites. Likewise, we only need a basis of two π orbitals $|1\rangle$ and $|2\rangle$. From the Hückel model we know that

$$E_0(d) = \langle 1|H_E|1\rangle \approx E_\pi - \langle 1|\frac{Z_{\text{eff}}e^2}{|\mathbf{r}-\mathbf{r}_2|}|1\rangle, \quad E_\pi = \langle 1|\left(\frac{\mathbf{p}^2}{2m} - \frac{Z_{\text{eff}}e^2}{|\mathbf{r}-\mathbf{r}_1|}\right)|1\rangle, \tag{B2}$$

where $d = |\mathbf{d}|$. Furthermore, $\mathbf{d}$ is the deviation from the equilibrium position of these neighbors and E_π is the ionization energy of the π bond. We proceed with

$$E_0(d) - E_\pi = Z_{\text{eff}}e^2\int dV\,\frac{|\psi_\pi(\mathbf{r}-\mathbf{r}_1)|^2}{|\mathbf{r}-\mathbf{r}_2|}, \tag{B3}$$

where $\psi_\pi(\mathbf{r}-\mathbf{r}_1)$ is the wave function of a π orbital centered at $\mathbf{r}_1$. We now recall that the nuclear variables engage in an oscillatory motion about an equilibrium position $\mathbf{R}$,

$$\mathbf{r}_2 - \mathbf{r}_1 - \mathbf{R} = \mathbf{d}, \tag{B4}$$

which allows us to substitute $\mathbf{r}_1$ in terms of $\mathbf{r}_2$:

$$E_0(d) - E_\pi = Z_{\text{eff}}e^2\int dV\,\frac{|\psi_\pi(\mathbf{r}-\mathbf{r}_2-\mathbf{R}-\mathbf{d})|^2}{|\mathbf{r}-\mathbf{r}_2|}. \tag{B5}$$

We note that the predominant part of the integrand is the region around $\mathbf{r}_2$, where the following approximation is valid:

$$|\boldsymbol{\eta}| \equiv |\mathbf{r}_2 - \mathbf{r}_1| \ll |\mathbf{R}+\mathbf{d}|. \tag{B6}$$

Therefore,

$$|\psi_\pi(\boldsymbol{\eta}+\mathbf{R}+\mathbf{d})| \approx |\psi_\pi(\boldsymbol{\eta})|e^{-|\mathbf{R}+\mathbf{d}|/\lambda}, \tag{B7}$$

which in turn yields the result

$$E_0(d) - E_\pi = \langle V\rangle\, e^{-2|\mathbf{R}+\mathbf{d}|/\lambda}, \quad \langle V\rangle = Z_{\text{eff}}e^2\int dV\,\frac{|\psi_\pi(\boldsymbol{\eta})|^2}{|\eta|}. \tag{B8}$$

Using the virial theorem, we can prove that $\langle V\rangle = 2E_0(d)$. On the other hand, we have the nearest-neighbor coupling

$$\Delta_0(d) = \langle 1|H_E|2\rangle \;= \int dV\,\psi_\pi^*(\mathbf{r}-\mathbf{r}_1)\left(\frac{\mathbf{p}^2}{2m} - \frac{Z_{\text{eff}}e^2}{|\mathbf{r}-\mathbf{r}_1|} - \frac{Z_{\text{eff}}e^2}{|\mathbf{r}-\mathbf{r}_2|}\right)\psi_\pi(\mathbf{r}-\mathbf{r}_2). \tag{B9}$$

This time, in order to employ (B7), we must focus on both regions centered around $\mathbf{r}_1$ and $\mathbf{r}_2$. After making the appropriate substitutions, it is straightforward to derive

$$\Delta_0(d) = 2e^{-|\mathbf{R}+\mathbf{d}|/\lambda}\left(E_0(d) - Z_{\text{eff}}e^2\int dV\,\frac{|\psi_\pi(\boldsymbol{\eta})|^2}{|\boldsymbol{\eta}+\mathbf{R}+\mathbf{d}|}\right). \tag{B10}$$

We can now expand our results in powers of $e^{-|\mathbf{R}+\mathbf{d}|/\lambda}$:

$$E_0(d) = E_\pi + \mathscr{O}_2\big(e^{-|\mathbf{R}+\mathbf{d}|/\lambda}\big), \quad \Delta_0(d) = \Delta(R)e^{-|\mathbf{R}+\mathbf{d}|/\lambda} + \mathscr{O}_2\big(e^{-|\mathbf{R}+\mathbf{d}|/\lambda}\big). \tag{B11}$$

By comparing the lowest-order correction due to nuclear observables in the diagonal and off-diagonal elements, we immediately see that $e^{-2|\mathbf{R}+\mathbf{d}|/\lambda} \ll e^{-|\mathbf{R}+\mathbf{d}|/\lambda}$. Finally, it is acceptable to introduce such a correction only in the off-diagonal terms.

[1] M. Born and R. Oppenheimer, Zur quantentheorie der molekeln, Ann. Phys. (Leipzig) **389**, 457 (1927).

[2] D. R. Hartree, On some approximate numerical applications of Bohr's theory of spectra, Cambridge Philos. Soc. **21**, 625 (1923).

[3] D. R. Hartree, The wave mechanics of an atom with a non-Coulomb central field. Part I. Theory and methods, Math. Proc. Cambridge Philos. Soc. **24**, 89 (1928).

[4] N. Argaman and G. Makov, Density functional theory: An introduction, Am. J. Phys. **68**, 69 (2000).

[5] A. Zangwill, Hartree and Thomas: The forefathers of density functional theory, Arch. Hist. Exact Sci. **67**, 331 (2013).

[6] A. Zangwill, The education of Walter Kohn and the creation of density functional theory, Arch. Hist. Exact Sci. **68**, 775 (2014).

[7] H. Kono, Y. Li, R. Zanasi, G. Monaco, F. F. Summa, L. T. Scott, A. Yagi, and K. Itami, Methylene-Bridged [6]-, [8]-, and [10] Cycloparaphenylenes: Size-dependent properties and paratropic belt currents, J. Am. Chem. Soc. **145**, 8939 (2023).

[8] L. Adamska, I. Nayyar, H. Chen, A. K. Swan, N. Oldani, S. Fernandez-Alberti, M. R. Golder, R. Jasti, S. K. Doorn, and S. Tretiak, Self-trapping of excitons, violation of Condon approximation, and efficient fluorescence in conjugated cycloparaphenylenes, Nano Lett. **14**, 6539 (2014).

[9] S. Reineke, M. Thomschke, B. Lüssem, and K. Leo, White organic light-emitting diodes: Status and perspective, Rev. Mod. Phys. **85**, 1245 (2013).

[10] C. Keum, C. Murawski, E. Archer, S. Kwon, A. Mischok, and M. C. Gather, A substrateless, flexible, and water-resistant organic light-emitting diode, Nat. Commun. **11**, 6250 (2020).

[11] S. H. Simon, *The Oxford Solid State Basics* (Oxford University Press, London, 2013).

[12] C. Kittel and P. McEuen, *Introduction to Solid State Physics* (Wiley, New York, 2018).

[13] N. Aravantinos-Zafiris, M. M. Sigalas, M. Kafesaki, and E. N. Economou, Phononic crystals and elastodynamics: Some relevant points, AIP Adv. **4**, 124203 (2014).

[14] B. W. Shore and P. L. Knight, The Jaynes-Cummings model, J. Mod. Opt. **40**, 1195 (1993).

[15] E. Mount, S.-Y. Baek, M. Blain, D. Stick, D. Gaultney, S. Crain, R. Noek, T. Kim, P. Maunz, and J. Kim, Single qubit manipulation in a microfabricated surface electrode ion trap, New J. Phys. **15**, 093018 (2013).

[16] J. M. Pino, J. M. Dreiling, C. Figgatt, J. P. Gaebler, S. A. Moses, M. S. Allman, C. H. Baldwin, M. Foss-Feig, D. Hayes, K. Mayer, C. Ryan-Anderson, and B. Neyenhuis, Demonstration of the trapped-ion quantum CCD computer architecture, Nature (London) **592**, 209 (2021).

[17] L. Xue, H. Yamazaki, R. Ren, M. Wanunu, A. P. Ivanov, and J. B. Edel, Solid-state nanopore sensors, Nat. Rev. Mater. **5**, 931 (2020).

[18] S. Schmid, P. Stömmer, H. Dietz, and C. Dekker, Nanopore electro-osmotic trap for the label-free study of single proteins and their conformations, Nat. Nanotechnol. **16**, 1244 (2021).

[19] S. Karmakar, S. Mondal, and B. Mandal, Eigensolutions of cyclopolyacene graphs, Mol. Phys. **113**, 719 (2015).

[20] E. Sadurní, F. Leyvraz, T. Stegmann, T. H. Seligman, and D. J. Klein, Hidden duality and accidental degeneracy in cycloacene and Möbius cycloacene, J. Math. Phys. **62**, 052102 (2021).

[21] G. Hall, On the eigenvalues of molecular graphs, Mol. Phys. **33**, 551 (1977).

[22] G. Hall, A graphical model of a class of molecules, Int. J. Math. Educ. Sci. Technol. **4**, 233 (1973).

[23] E. Hückel, Quantentheoretische beiträge zum benzolproblem, Z. Phys. **70**, 204 (1931).

[24] E. Hückel, Quantentheoretische beiträge zum benzolproblem, Z. Phys. **72**, 310 (1931).

[25] P. W. Atkins and R. S. Friedman, *Molecular Quantum Mechanics*, 5th ed. (Oxford University Press, London, 2010).

[26] Y. Hernández-Espinosa, R. A. Méndez-Sánchez, and E. Sadurní, On the electronic structure of benzene and borazine: An algebraic description, J. Phys. B **53**, 105101 (2020).

[27] I. D. Clark and D. C. Frost, A study of the energy levels in benzene and some fluorobenzenes by photoelectron spectroscopy, J. Am. Chem. Soc. **89**, 244 (1967).

[28] E. Tegeler, G. Wiech, and A. Faessler, X-ray spectroscopic study of the electronic structure of benzene, monofluoro- and monochlorobenzene, J. Phys. B **13**, 4771 (1980).

[29] National Institute of Advanced Industrial Science and Technology, Japan, Spectral database for organic compounds, SDBS, https://sdbs.db.aist.go.jp (1999).

[30] B. C. Smith, Group wavenumbers and an introduction to the spectroscopy of benzene rings, Spectroscopy **31**, 34 (2016).

[31] V. I. Man'ko, G. Marmo, E. C. G. Sudarshan, and F. Zaccaria, f-oscillators and nonlinear coherent states, Phys. Scr. **55**, 528 (1997).

[32] E. Sadurní and E. Rivera-Mociños, Fractal position spectrum for a class of oscillators, J. Phys. A: Math. Theor. **48**, 405301 (2015).

[33] P. M. Morse, Diatomic molecules according to the wave mechanics. II. Vibrational levels, Phys. Rev. **34**, 57 (1929).

[34] B. W. Shore, Comparison of matrix methods applied to the radial Schrödinger eigenvalue equation: The morse potential, J. Chem. Phys. **59**, 6450 (1973).

[35] J. J. Sakurai, *Modern Quantum Mechanics*, 1st ed. (Addison-Wesley, Reading, 1994).

[36] K. Zhao, M. Zhao, Z. Wang, and Y. Fan, Tight-binding model for the electronic structures of SiC and BN nanoribbons, Physica E **43**, 440 (2010).

[37] E. N. Koukaras, G. Kalosakas, C. Galiotis, and K. Papagelis, Phonon properties of graphene derived from molecular dynamics simulations, Sci. Rep. **5**, 12923 (2015).

[38] F. Ramírez-Ramírez, E. Flores-Olmedo, G. Báez, E. Sadurní, and R. A. Méndez-Sánchez, Emulating tightly bound electrons in crystalline solids using mechanical waves, Sci. Rep. **10**, 10229 (2020).

[39] K. Shioya, K. Mishima, and K. Yamashita, Quantum computing using molecular vibrational and rotational modes, Mol. Phys. **105**, 1283 (2007).